Impact of Aerosols on IASI Observations

Michel Kruglanski - Martine De Maziere
Michel.Kruglanski@oma.be

Belgian Institute for Space Aeronomy (BIRA-IASB)
Avenue circulaire, 3, Ringlaan
Brussels, 1180, Belgium

ABSTRACT

This paper summarizes the research activity carried out at the Belgian Institute for Space Aeronomy in the framework of the CNES/EUMETSAT project called 'Chemistry and Climate related studies using the IASI remote sensor' (PI: Dr. C. Clerbaux, IPSL/CNRS). IASI stands for Infrared Atmospheric Sounding Interferometer, a Michelson interferometer-type instrument that is part of the METOP-1 payload, to be launched in 2005 in a polar sun-synchronous orbit at 840 km altitude. The present research focuses on the feasibility of retrieving aerosol properties from the IASI spectra. It contributes to the development of scientific retrieval algorithms for IASI, to derive concentrations of atmospheric molecular species, like O_3, CH_4, and CO, and, if feasible, of aerosol properties.

INTRODUCTION

The presence of aerosols modifies infrared radiances at the top of the atmosphere through an increase of the atmospheric absorption. Retrievals of atmospheric parameters from nadir infrared radiance measurements can be affected by occurrence of significant aerosol concentrations. Examples are Sahara dust advection over the ocean, biomass burning in the tropics and volcanic aerosols from a major eruption. Therefore, in the framework of a project concerning the development of retrieval algorithms for minor atmospheric compounds, we investigate the sensitivity of the IASI spectral radiance measurements to the presence and the type of aerosol. IASI is a Michelson interferometer operating in the thermal infrared to perform atmospheric nadir-viewing emission measurements, as part of the operational payload of the polar satellite series METOP. In addition to its operational meteorological mission, IASI has atmospheric research objectives including the retrieval of H_2O, CO, O_3, CH_4 and N_2O column amounts and vertical profiles. The launch of the first satellite is planned for 2005.

For the spectral range of the IASI instrument, the radiance at the top of atmosphere as a function of wavenumber ν merely reads

$$L = \varepsilon_0 \, B(\nu, T_{surf}) \exp[\, -\sigma_{0\infty} \,] \; + \; \int dz \; B(\nu, T_z) \exp[\, -\sigma_{z\infty} \,] \qquad (1)$$

in which the two terms correspond to the surface emission and the thermal emission added along the atmospheric path, respectively. Hereinafter, we will designate the latter part by path thermal emission. The surface emission results from the black body radiance of the surface at temperature T_{surf}, modulated by the surface emissivity ε_0, and attenuated by the total optical depth $\sigma_{0\infty}$ of the atmosphere. The spectral dependence of $\varepsilon_0$has been omitted from the formula, for the sake of simplicity. The path thermal emission term is the integral of the radiances originating in each atmospheric layer. For each layer, the radiance is attenuated by optical depth $\sigma_{z\infty}$ of the layers above. In Figure 1, a typical radiance spectrum is shown at a resolution of 2 cm^{-1}. It has been obtained with the MODTRAN code [Kneizys et al., 1996] using atmospheric profiles from the 1976 US Standard Atmosphere, a 300K ocean surface emissivity and no aerosol contamination. The spectral range has been subdivided according to the three bands of the IASI instrument: 645-1210, 1210-2000 and 2000-2760 cm^{-1}, respectively. The colour scale emphasizes the relative contributions of both the surface emission and the path thermal emission. In blue regions, the path thermal emission is dominant and the radiance should be rather independent of the conditions near the surface. The red regions are atmospheric windows for which the surface emission is the major term.

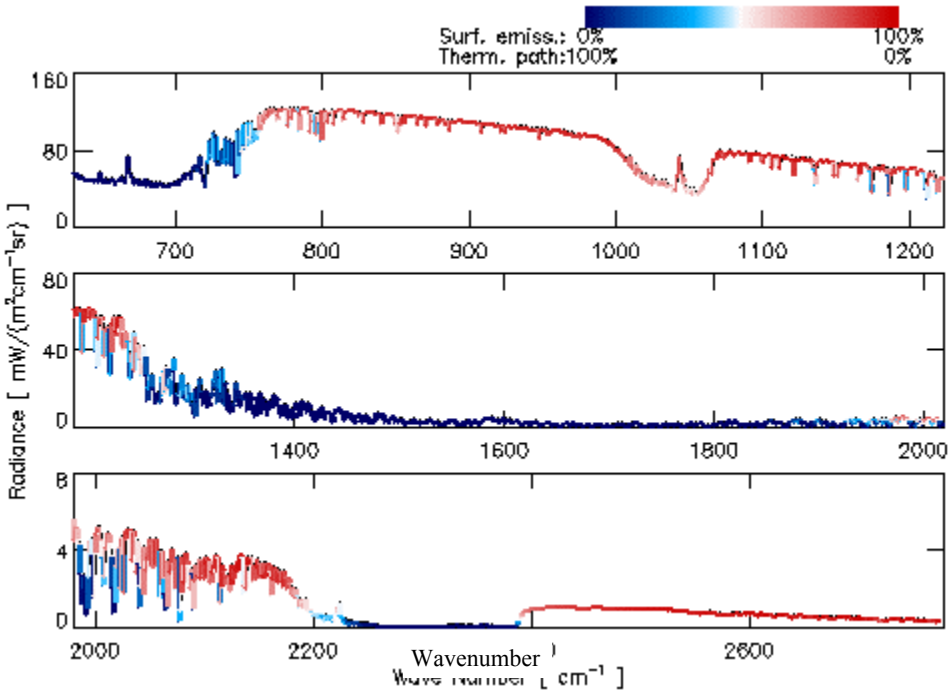

Figure 8: Radiance spectrum at the top of atmosphere in the case of a 1976 US Standard Atmosphere and a 300K ocean surface. The colour scale indicates the relative contributions of the surface emission (reddish) and the path thermal emission (bluish).

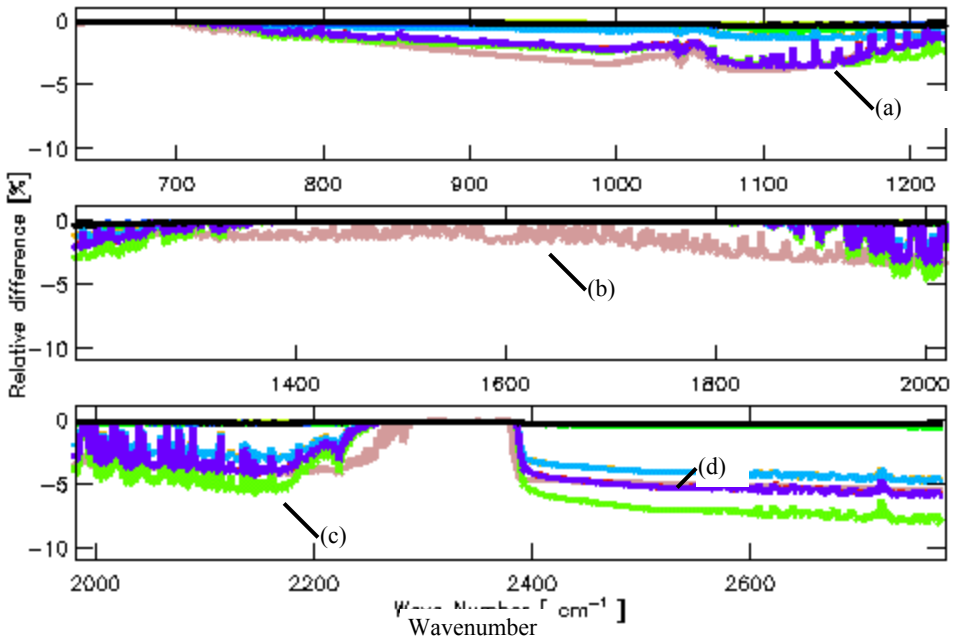

Figure 9: Relative variations of the radiance spectrum at the top of atmosphere due to the presence of different aerosol populations for the same atmospheric and surface conditions as in Fig. 1: (a) rural aerosols with a visibility of 5 km, (b) fresh high stratospheric volcanic aerosols, (c) urban aerosols with a visibility of 5 km, (d) maritime aerosols with a visibility of 23 km.

The presence of aerosols affects the radiance at the top of atmosphere by modifying the atmospheric optical depth. The MODTRAN code includes several models of aerosol populations and can be used to evaluate their impact. In Figure 2, the impact of aerosols is illustrated for the atmospheric and surface conditions of Fig. 1. Each curve corresponds to the radiance variance due to a different kind of aerosol population. Except for one case, the aerosol impact occurs mainly inside the atmospheric windows. The exception corresponds to a population of fresh volcanic stratospheric aerosols. The other significant variations are due to aerosol populations located in the boundary layer (0 to 2 km of altitude), e.g. rural aerosol with a visibility of 5 km.

Since stratospheric aerosol can be detected almost only in case of a high, fresh volcanic aerosol load, we focus our study on the low-altitude aerosols. To identify the atmospheric and/or surface parameters that determine the sensitivity to the aerosols, we first develop a simple analytical formulation of the radiance variation for the case of nadir atmospheric observations. Using ECMWF parameters, we are then able to produce global maps giving an indication of the sensitivity of IASI-like spectra to aerosol in the planetary boundary layer. We also started the development of an algorithm to extract aerosol information from IASI spectral observations.

RESULTS

For a nadir viewing geometry, we have shown that the radiance of Eq. (1), in the presence of aerosol can be approximated by

$$L \approx L_0 + \Delta\sigma \left\{ B(\nu,T_0) - \varepsilon_0 B(\nu,T_{surf}) \right\} \exp[-\sigma_{0\infty}] \qquad (2)$$

if the aerosol population is confined in a thin layer in the planetary boundary layer. In Eq. (2), L_0 is the radiance in absence of aerosol, $\Delta\sigma$ is the variation of the total optical thickness of the atmosphere due to the presence of aerosols, and T_0 is the temperature of the atmospheric layer holding the aerosol population. In the second term of this equation, only the first factor is function of the aerosols. The last factor corresponds to the total transmission of the atmosphere in absence of aerosols, and the middle factor clearly shows that the temperature contrast between the surface and the aerosol layer plays a major role in determining the impact of aerosols on nadir observations of the thermal radiance. In Figure 3, the simple formulation of Eq. (2) is illustrated in the case of a contamination of the radiance by a load of rural aerosol with 5 km visibility, with atmospheric and surface conditions that are the same ones as in Figure 1. From top to bottom, the first panel show the radiance L_0 already presented in Fig. 1. The radiance variation $L - L_0$ simulated with MODTRAN is presented on the second panel (green curve), as well as the separate contributions of the surface emission and the path thermal emission. The next three panels display the three distinct factors of Eq. (2): the temperature contrast factor, the optical thickness variation caused by rural aerosols and the total transmission of a clean atmosphere, respectively. The product of the three factors is successfully confronted with the simulated radiation variation on the last panel where the enclosed panel shows the approximation error for the spectral range 645-1210 cm^{-1}. The formulation of Eq. (2) has been verified successfully for different aerosol cases in a similar way.

Figure (3) also shows that the spectral interval between 700 and 1200 cm-1 offers the best sensitivity to aerosol, mainly because the temperature contrast factor decreases with wavenumber. In this spectral range, only O_3, H_2O and CO_2 have significant absorptions, which are constituted by single line absorptions and continuum contributions. This is the reason why further onwards, the work focuses on this spectral interval, i.e., the first IASI band.

Aerosol sensitivity maps

The formulation of Eq. (2) shows that the product of its last two factors,

$$\mathcal{F} = \left\{ B(\nu_x,T_0) - \varepsilon_0 B(\nu_x,T_{surf}) \right\} \exp[-\sigma_{0\infty}] \qquad (3)$$

provides a measure of the sensitivity of the observation to aerosols, under the assumptions outlined above. The factor $\mathcal{F}$ can be evaluated at a specific wavenumber ν_x using surface and atmospheric parameters either retrieved from operational observations or generated by forecasting models. To illustrate this capability, we evaluate $\mathcal{F}$ using data from the operational atmospheric model daily archive of the European Centre for Medium-Range Weather Forecasts (ECMWF, http://www.ecmf.int). The ECMWF data include the profiles, on 15 pressure levels, of the atmospheric temperature, relative humidity and geopotential height, the temperature of the surface and just above the surface, and the surface pressure. All the data are available on a grid of one by one degree in latitude and longitude, and with a time step of 6

hours. The factor $\mathcal{F}$ has been evaluated by identifying T_0 as the temperature at 2 km altitude, neglecting the surface emissivity spectral dependence and restricting $\sigma_{0\infty}$ to the water-vapour continuum contribution, which corresponds to the main shape of the optical depth in the atmospheric window. From the ECMWF data, 4 world maps per day showing the sensitivity of IASI-type spectra to the presence of low-altitude aerosol can be produced.

In order to reduce the number of maps and to increase their practicability, the world maps are projected on the spacecraft orbit. Since the METOP platforms will be launched in a helio-synchronous orbit, the projection is reduced to a daily map for each orbit leg. Such maps are presented in Figs. 4 and 5 for June 16, 1997. The factor $\mathcal{F}$ is evaluated at 800 cm^{-1} along the ascending leg and at 1175 cm^{-1} along the descending leg, respectively. Both figures display the sensitivity factor $\mathcal{F}$ as well as the two distinct factors of Eq. (3) separately. The maps allows to determine the orbit parts either where the infrared radiance observations are free of low-altitude aerosol contaminations, or where information about low-altitude aerosols can be retrieved from these observations.

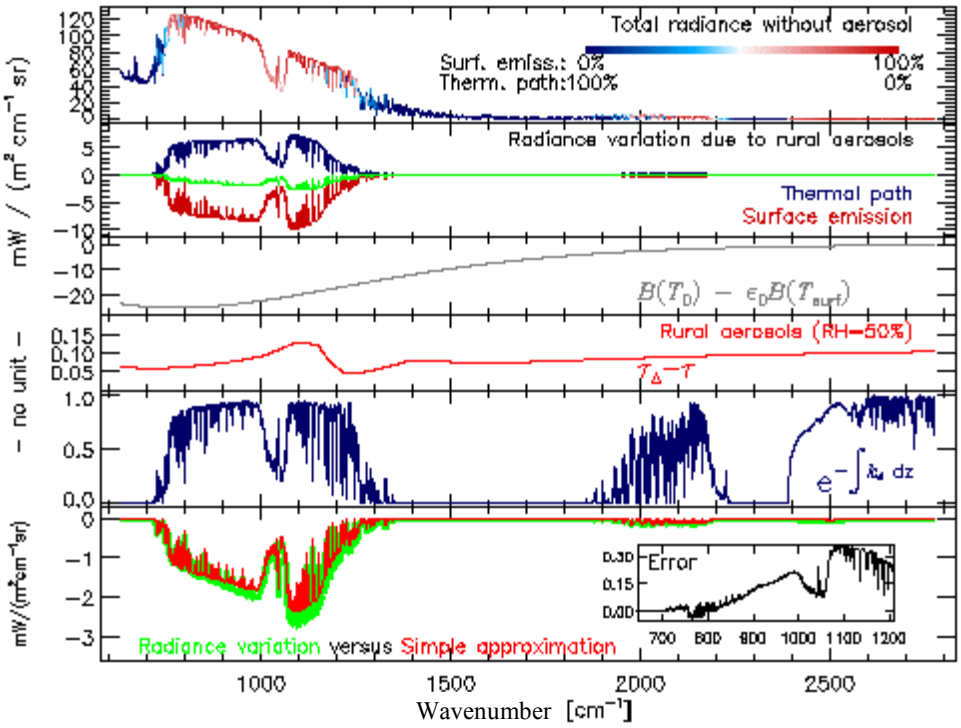

Figure 10: Validation of the analytical approximate Eq. (2) for evaluating the impact of low-altitude aerosols on nadir viewing infrared radiance. From top to bottom: radiance spectrum for the same conditions as Fig. 1; variation of the path thermal emission, surface emission and total radiance due to an atmospheric load of rural aerosols; temperature contrast factor; aerosol optical thickness; total transmission of the aerosol-free atmosphere; confrontation of simulated radiance (MODTRAN) with the corresponding approximate evaluation from Eq. (2).

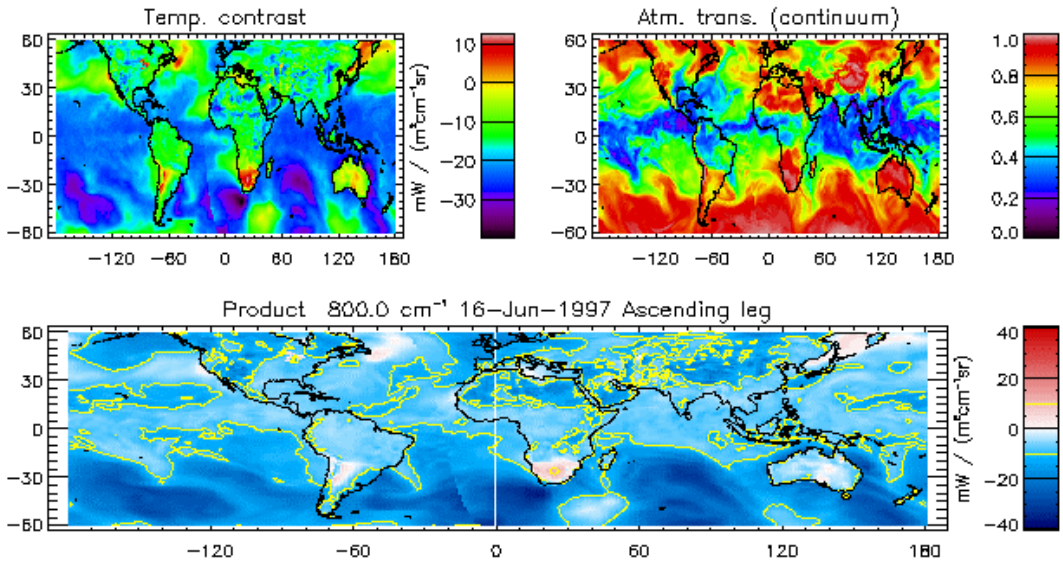

Figure 11: Temperature contrast factor, atmospheric total transmission and low-altitude aerosol sensitivity maps at 800 cm-1 projected on ascending legs of an helio-synchronous orbit (10:30 ascending node crossing time). The maps are based on ECMWF data for June 16, 1997

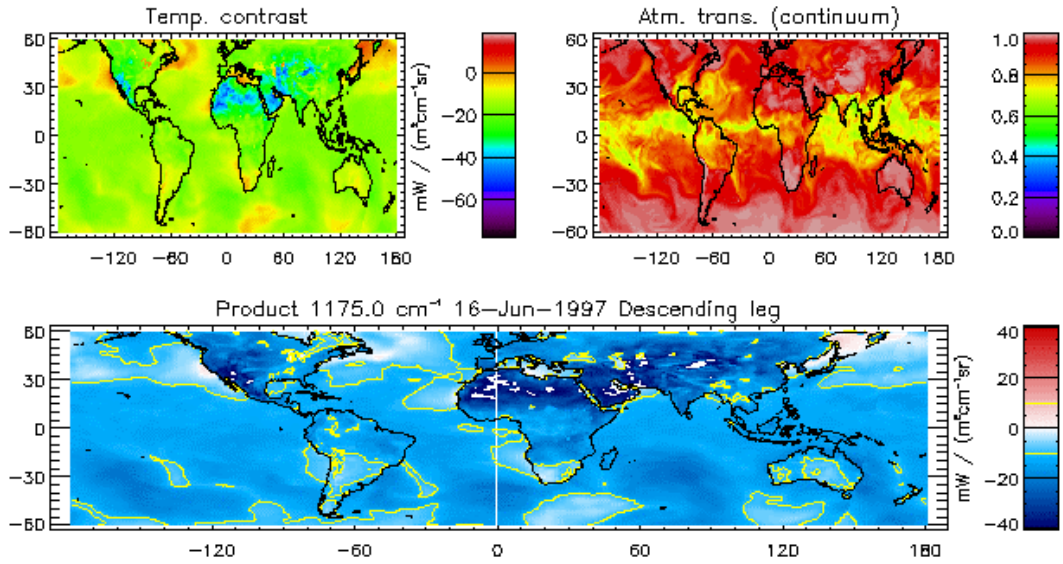

Figure 12: Same as Fig. 4, but evaluated at 1175 cm^{-1} and projected on descending legs of an helio-synchronous orbit (10:30 ascending node crossing time).

Low-resolution evaluation of the molecular absorption coefficients

When operational, IASI measurements will be used to retrieve vertical profiles of atmospheric components like H_2O and O_3. The retrieval algorithms for molecular species are based mainly on the shape of several narrow absorption lines. On the contrary, aerosol absorption signatures are spectrally broad, allowing the differentiation with respect to the molecular features.

We have investigated a strategy to compare the infrared radiance observations to synthetic spectral radiances in order to retrieve aerosol information, exploiting the different spectral behaviours of the aerosol and molecular components. The proposed strategy is based on an iterative algorithm where the aerosol optical depth is adjusted to make the synthetic and observed radiances agree. We plan to compare both radiances at a low spectral resolution by selecting a set of wavenumbers ν_i as distant as possible of the molecular multiple narrow absorption lines. The algorithm is illustrated in Fig. 6. The inputs are: the vertical profiles of temperature, pressure and atmospheric components, the surface temperature and emissivity, the viewing and Sun zenith angles, and the radiances at ν_i. The number of interfering molecular

species is limited to essentially three components (O_3, H_2O and CO_2) since we are dealing with the 700-1200 cm^{-1} range. The inputs are expected to be retrieved from IASI and other instruments aboard the METOP platform. The final result is the total optical depth of the aerosols at ν_i. When developed, the algorithm will be tested using data from the instrument IMG aboard ADEOS, that has been operational between October'96 and June'97.

The algorithm requires the evaluation of the optical depths of the atmospheric components from the retrieved vertical profiles and the molecular absorption coefficients. In order to speed up the algorithm, we have developed a low spectral resolution technique similar to the band model ones [Goody and Yung, 1989]. The technique assumes a selection of the ν_i such that the shape of molecular absorption lines reduces to the asymptotic wings of the Lorentz [1906] line shapes. In that case, two effective Lorentz lines are sufficient to simulate the ensemble of absorption lines of each atmospheric component. Moreover, the Lorentz line parameters do not depend on the atmospheric pressure. An application to H_2O absorption when ν_i = 780 cm^{-1} is illustrated in Fig. 7. On the left panel, the H_2O molecular absorption coefficient (solid green curve) is evaluated in the range $\nu_i \pm 25$ cm^{-1} by a sum of Lorentz lines, the parameter of which are extracted from the HITRAN database [Rothman et al., 1992]. In this interval, the whole absorption near 780 cm^{-1}due to the lines centred on a wavenumber lower than ν_i is emulated by the absorption of a single effective Lorentz line (red curve). The second Lorentz line (blue curve) emulates the absorption of the lines centred on a wavenumber higher than ν_i. On the upper right panel, both exact and effective absorption coefficients are nicely compared in the vinicity of 780 cm^{-1}, for the left and right lines separately, as well as for the combined absorption. In the range $\nu_i \pm$ ½ cm^{-1}, the difference is lower than 1%. One should remember that the technique is valid only if the ν_i is not enclosed in an absorption line of the concerned molecule.

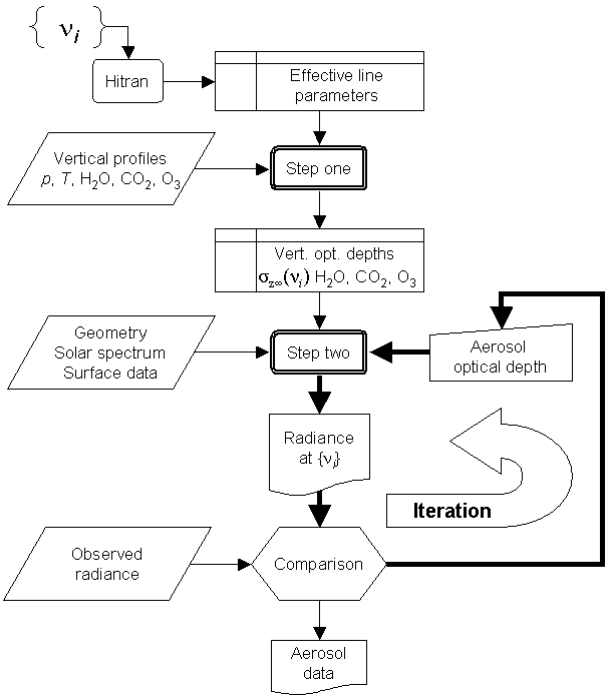

Figure 13: Iterative algorithm to retrieve low-altitudes aerosol information from IASI radiance measurements.

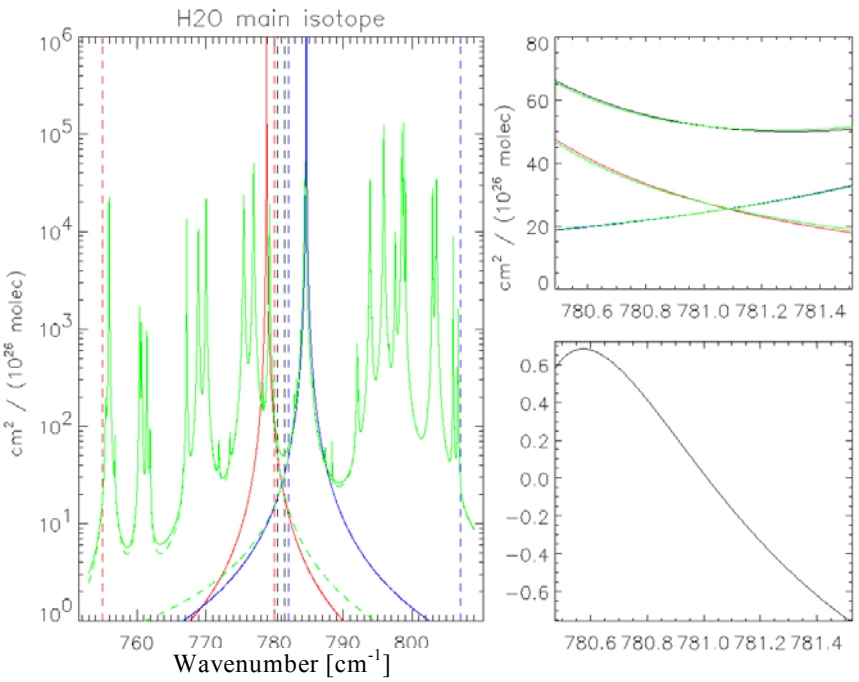

Figure 14: Technique using two effective Lorentz lines for the evaluation of molecular absorption coefficient, demonstrated for the H_2O molecule at standare pressure and temperature conditions (296K, 1atm) in the vicinity of 780 cm^{-1}. The lower right panel shows the absolute error of the approximation.

CONCLUSIONS

IASI, Infrared Atmospheric Sounding Interferometer, will make nadir observations of the thermal radiance spectra from the Earth atmosphere system. It will be launched on METOP-1 in 2005.
In a first phase reported here, the research activities at BIRA-IASB that are performed specifically in the frame of the project 'Chemistry and Climate related studies using the IASI remote sensor' have focused on a theoretical investigation of the sensitivity of IASI spectra to aerosol. It has been demonstrated that the highest sensitivity occurs for low altitude aerosol. A fast operational algorithm has been designed for the retrieval of aerosol properties from IASI-like spectra.
In the next phase, this algorithm will be implemented and tested using available IMG/ADEOS spectra.

ACKNOWLEDGEMENTS

The authors wish to thank R. Van Lierde and J.-C. Jodogne of the Royal Institute of Meteorology (IRM/KMI) for providing access to the ECMWF archive. The study is funded by the PRODEX programme [ESA Contract 13582/99/NL/VJ(IC)].

REFERENCES

Goody R.M. and Y.L. Yung, Atmospheric Radiation Theoretical basis, Oxford University press, New York, 1989.
Kneizys F.X. et al., The MODTRAN 2/3 Report and LOWTRAN 7 Model, NrF19628-91-C-0132, 1996.
Lorentz, H.A., the absorption and emission of lines of gaseous bodies, proc. R. Acad. Sci. (Amsterdam) 8, 591, 1906.
Rothman L.S. et al., The HITRAN molecular database: editions of 1991 and 1992, Journal of Quantitative Spectroscopy and Radiative Transfer 48, 496, 1992.

ADDENDUM

M. Kruglanski has attended the Ecole d'été internationale, Interactions Aérosols, Nuages et Rayonnement, CNES, FRANCE, 16–28 September 2001.